 https://doi.org/10.3311/PPci.23961

Periodica Polytechnica Civil Engineering, 68(3), pp. 742–754, 2024

Failure Mechanism and Structural Safety Assessment of the Primary Support Structure of Soft Rock Tunnel: A Case Study

Jing Chen[1*], Yong Hua Ding[1], Yi Fu Liu[2], Zhou Shi[3]

[1] Department of Architecture Engineering, Zhengzhou University of Industrial Technology, No 16 Xueyuan Road, Xinzheng City, Zhengzhou 451100, Henan, China
[2] School of Emergency Management and Safety Engineering, China University of Mining and Technology (Beijing), Beijing 100083, China
[3] Department of Geotechnical Engineering, College of Civil Engineering, Tongji University, Shanghai 200092, China
[*] Corresponding author, e-mail: 003520@zzuit.edu.cn

Received: 27 November 2023, Accepted: 26 December 2023, Published online: 14 March 2024

Abstract

Based on a soft rock tunnel in a mountainous area of northwest Yunnan Province, a refined numerical model of different support forms considering structural interaction is established to comprehensively evaluate the structural failure mechanisms and mechanical responses of different support forms. Research shows that compared to steel rib structures, the axial force and bending moment of sprayed concrete structures is larger under different combinations of support structures. Compared with a single-layer support structure, the stress distribution at each position of the double-layer I-shaped steel structure is more uniform, and the sprayed concrete structure only experiences compression damage at the corner of the side wall. As the strength of sprayed concrete increases, the stress distribution of sprayed concrete at the arch waist becomes more uniform. The stress concentration state of sprayed concrete at the corner of the tunnel wall and the plastic yield state of the steel rib structure have also been improved. The higher the concrete strength, the lower the stress ratio on the steel rib's inner and outer sides.

Keywords

tunnel engineering, support structure, structural optimization, mechanical properties, safety assessment

1 Introduction

With the rapid development of the western region and the continuous extension of new land-sea channels, Yunnan Province, as an important port for China's foreign trade, has entered a new stage of development in transportation infrastructure such as highways [1, 2]. With the rapid development of transportation in mountainous areas, many tunnel projects have been constructed, posing great challenges in safely and efficiently crossing areas with compressible surrounding rocks [3, 4]. Especially in the mountainous areas of western Yunnan, there is a large amount of mixed rock of carbonaceous slate and phyllite, with loose rock structure and poor stability. In addition, the regional tectonic stress is strong, and the problem of large deformation of soft rock during tunnel crossing in this area is particularly prominent [5–8].

Many experts and scholars have achieved certain research results on the field application and engineering effects of double or multi-layer primary support structures in soft rock tunnels [9–16]. However, many studies mainly rely on field tests with high cost. Most studies mainly evaluate and determine the safety and stability of the structure from the perspectives of surrounding rock pressure, support structure stress, etc. Due to limited field engineering conditions, the amount of field test data is limited and the research scope involved is relatively limited [9, 17, 18]. The numerical calculation model derived from field tests can overcome the research difficulties of single field test conditions and the difficulty in obtaining refined structural data [5, 19–21]. However, in the past, when establishing support structure models for large deformation tunnels in soft rock, sprayed concrete and steel rib structures with significant differences in stiffness and physical and mechanical properties in the primary support structure were often equivalent to uniform structures, which makes the mechanical response of the support structure in the numerical model significantly different from the field situation, and it is also impossible to compare and analyze

Cite this article as: Chen, J., Ding, Y. H., Liu, Y. F., Shi, Z. "Failure Mechanism and Structural Safety Assessment of the Primary Support Structure of Soft Rock Tunnel: A Case Study", Periodica Polytechnica Civil Engineering, 68(3), pp. 742–754, 2024. https://doi.org/10.3311/PPci.23961

the mechanical response and damage mechanism of sprayed concrete and steel rib structures under different primary support combinations, and cannot provide precise guidance for engineering practice [22]. Therefore, it is necessary to establish a refined numerical calculation model based on field tests to truly reproduce the combination method of field support structures and to timely supplement and provide positive feedback on the evaluation results of field experimental data, to comprehensively analyze the structural mechanical response and failure mechanism in soft rock tunnels.

Based on a soft rock tunnel in a mountainous area of northwest Yunnan Province, through field tests, this study analyzes the deformation characteristics of the tunnel and the mechanical response of the support structure under different support forms. Then, a refined numerical analysis model of different support forms considering structural interaction is established for soft rock tunnels, to comprehensively evaluate the structural failure mechanisms and mechanical responses of different support forms in soft rock tunnels, to provide a reference for the prevention and control of large deformation disasters in soft rock tunnels and the selection of support structure forms.

2 Geological condition and geostress testing

2.1 Engineering overview

The supporting project is located in the northwest of Yunnan Province, with complex terrain and geological conditions along the line. It has the "three highs" characteristics of high altitude, high seismic intensity, and high ground stress. The lithology is weak and fragmented, and active faults are developed, making tunnel construction safety risks extremely high. The direction of the rock layer intersects with the tunnel axis at a small angle. The rock mass is loose and fragmented, with poor interlayer bonding. Local bedding is disrupted by compression, and the compressive structural surface of the rock layer is smooth and straight. During the tunnel construction process, problems such as local steel rib distortion and local tunnel collapse occurred. The field rock layer joints and engineering disasters are shown in Fig. 1.

Fig. 1 The field rock layer joints and engineering disaster

2.2 Rock mass strength and deformation statistics

The soft rocks within the tunnel are mainly carbonaceous slate, phyllite, and carbonaceous shale, with extremely low rock strength and obvious rock cracks. The rock cores taken are mostly block-shaped, with uneven layers containing 5-10m thick moderately weathered carbonaceous mud plates. The rock mass is extremely fragmented, and the field rock mass point load test values along the tunnel are shown in Fig. 2.

From Fig. 2, it can be seen that the point load strength of the rock mass within a longitudinal range of 1200 meters in the tunnel exhibits a Gaussian distribution as a whole, with a maximum value of 4.2 MPa. To investigate the distribution of ground stress in the tunnel, the hydraulic fracturing method was used on the sidewall of the tunnel for ground stress testing. The elevation depth of the measuring point was 235 meters, and the maximum principal stress value at the measuring point position was 8.708 MPa. The strength-stress ratio of the large deformation section of the tunnel is 5.57, and the field stress level in the rock mass is in a high-stress state. Therefore, the tunnel surrounding the rock belongs to high-stress soft rock. To ensure construction safety and conduct a real-time evaluation of the dynamic deformation evolution law of surrounding rock, the settlement and convergence of surrounding rock in 80 large deformation sections of the tunnel were tested and analyzed, and the statistical results are shown in Fig. 3.

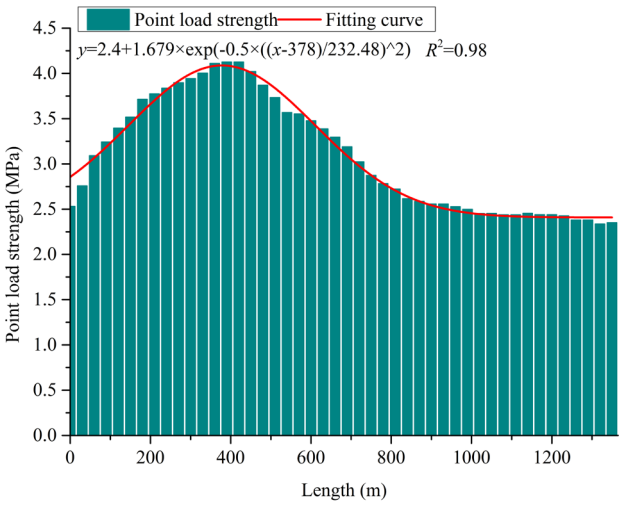

Fig. 2 Test values of point load strength of rock mass along tunnel

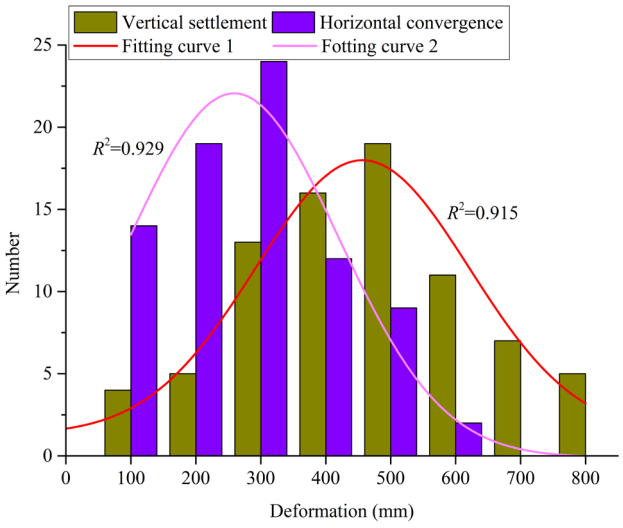

Fig. 3 Distribution of tunnel settlement and horizontal convergence in the large deformation section

From Fig. 3, it can be seen that the surrounding rock and primary support after tunnel excavation mainly rely on tunnel settlement, followed by the sidewall convergences. The relationship between deformation and frequency follows a Gaussian distribution, with arch settlement mainly concentrated between 300mm and 500mm, and horizontal convergence mainly concentrated between 100mm and 300mm. The engineering measure is that the reserved deformation has been increased during the tunnel construction process, and the primary support has been strengthened, that is, the single-layer primary support has been optimized to a double-layer primary support structure.

3 Field testing for different primary support forms

3.1 Evolution law of structure deformation

To study the mechanical behavior of structural construction under different forms of primary support structures in soft rock tunnels with large deformation, two test sections were arranged in the V-grade surrounding rock section, and two field tests were carried out with different support schemes. The primary support steel ribs used were single-layer I25b steel ribs, outer layer I25b steel ribs, and inner layer I20 steel ribs, respectively. The deformation and stress of the primary support of the tunnel under single-layer support structure and double-layer support structure were monitored. The test results of tunnel settlement under different support schemes are shown in Fig. 4.

As shown in Fig. 4, for a single-layer steel rib structure, the tunnel settlement is relatively large, with a maximum settlement of 397 mm, while the maximum settlement is about in 300 mm in double-layer primary support. The tunnel deformation is significantly affected by the excavation of every part of the tunnel, and the variation pattern of settlement at each monitoring point at the upper, middle, and lower benches is consistent. The deformation of this section increased sharply after the excavation of the upper

bench, and the deformation rate slowed down after the primary support construction of the middle bench. After the excavation of the lower bench, the deformation rate increases again, and the temporal curve shows a turning point, leading to rapid development of deformation.

3.2 Strain testing and analysis of steel rib structures

To visually present the strain of the steel rib at various positions in the tunnel, this study presents the strain at each position of the horseshoe-shaped steel arch structure in a circular shape. The angles of each measuring point are calibrated according to the angle between their actual position and the center of the tunnel circle. The internal and external strains of the steel rib structure under different support structure forms are shown in Fig. 5.

From Fig. 5 (a), it can be seen that the strain on the inner and outer sides of the steel rib in the single-layer I-beam support structure is positive, and the strain distribution of the steel rib on the inner and outer sides of the structure is extremely uneven. Both the inner and outer steel rib structures have significant strain on the right side of the structure, with the maximum strain on the inner side, 1060×10^{-6}, located at 75 degrees in the upper right corner, with a maximum strain of 1045×10^{-6} on the outer side, located at 90 degrees on the right side, with the maximum strain approaching 70% of the yield strain of the steel rib, indicating a low overall safety reserve of the structure.

While from Fig. 5 (b), it can be seen that in the double-layer I-beam support structure, the overall strain on

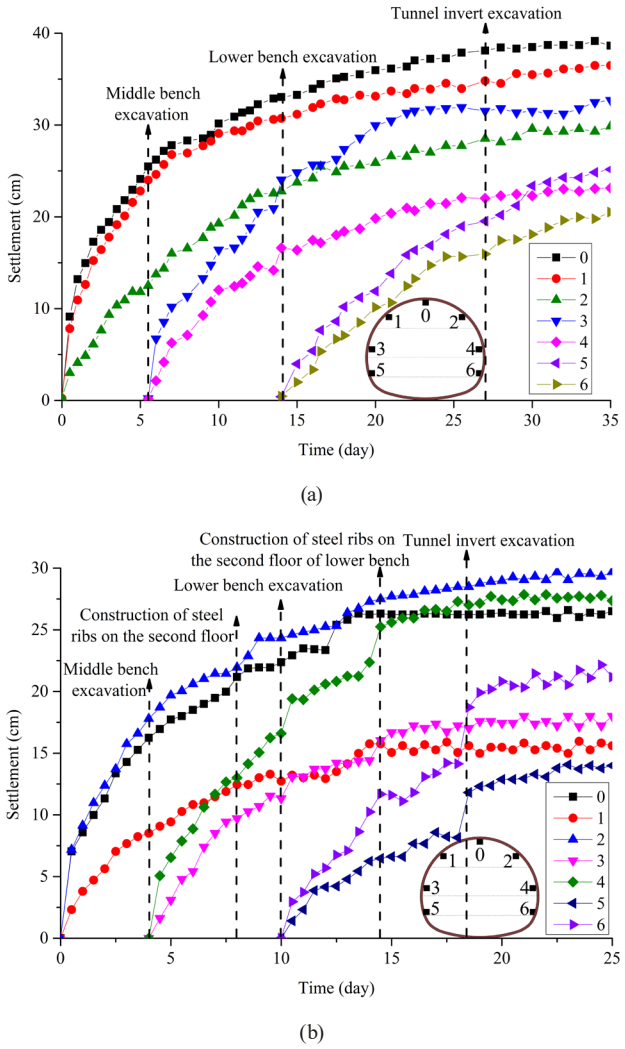

Fig. 4 Structural settlement test results under different support forms; (a) Single-layer primary support, (b) Double-layer primary support

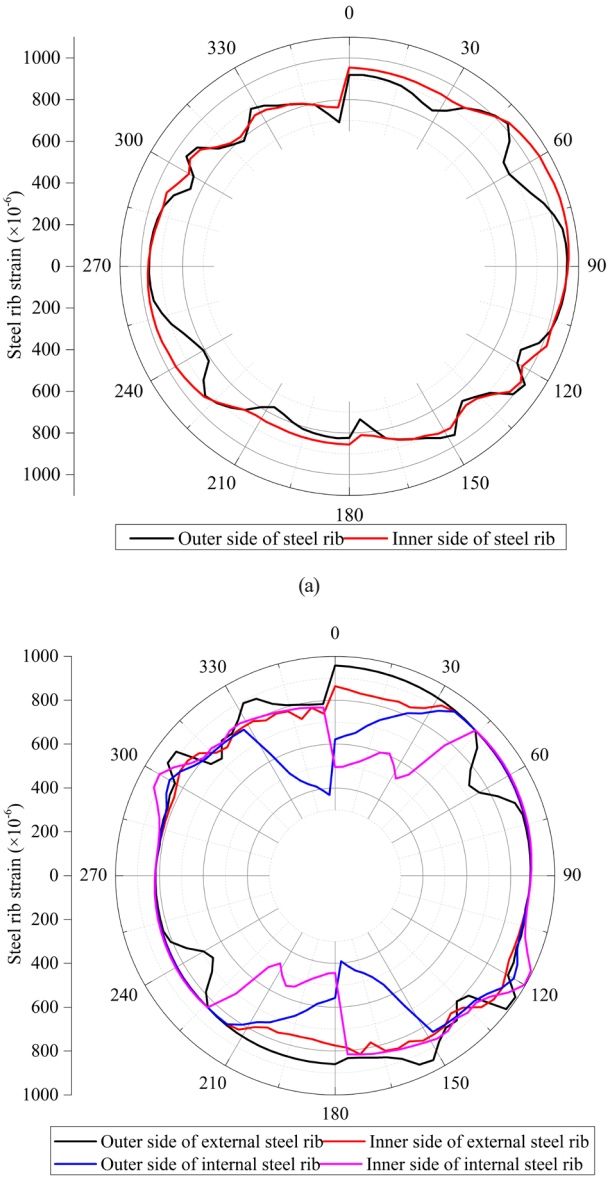

Fig. 5 Internal and external strains of steel rib under different support forms; (a) Single-layer primary support, (b) Double-layer primary support

the inner and outer sides of the inner steel rib is between 391 × 10-6-924 × 10^{-6} and 443 × 10^{-6}–996 × 10^{-6}, the average strain is 766 × 10^{-6} and 778 × 10^{-6} respectively, approximately 51% of the yield strain of the steel rib. The maximum and average strain of the steel rib under the support of the double-layer I-beam composite structure is less than that of the single-layer steel rib, and the structural strain is only about 50% of the limit value.

Overall, the combined bearing system composed of double-layer steel ribs can effectively avoid the deformation and invasion of the support structure caused by insufficient support strength and stiffness, as well as the large-scale instability and damage of the steel rib structure, compared to single-layer steel ribs. However, engineering practice has also shown that under significant compressive stress, the shotcrete at some positions of the double-layer support structure also experiences compressive damage and local peeling, posing significant risks to the long-term safety and stability of the support structure. Therefore, based on on-site engineering, this study analyzes the damage behavior and mechanical characteristics of tunnel support structures under different forms of support structures by numerical models, which can provide a reference for improving the safety and stability performance of structures in large deformation tunnels with squeezed surrounding rocks.

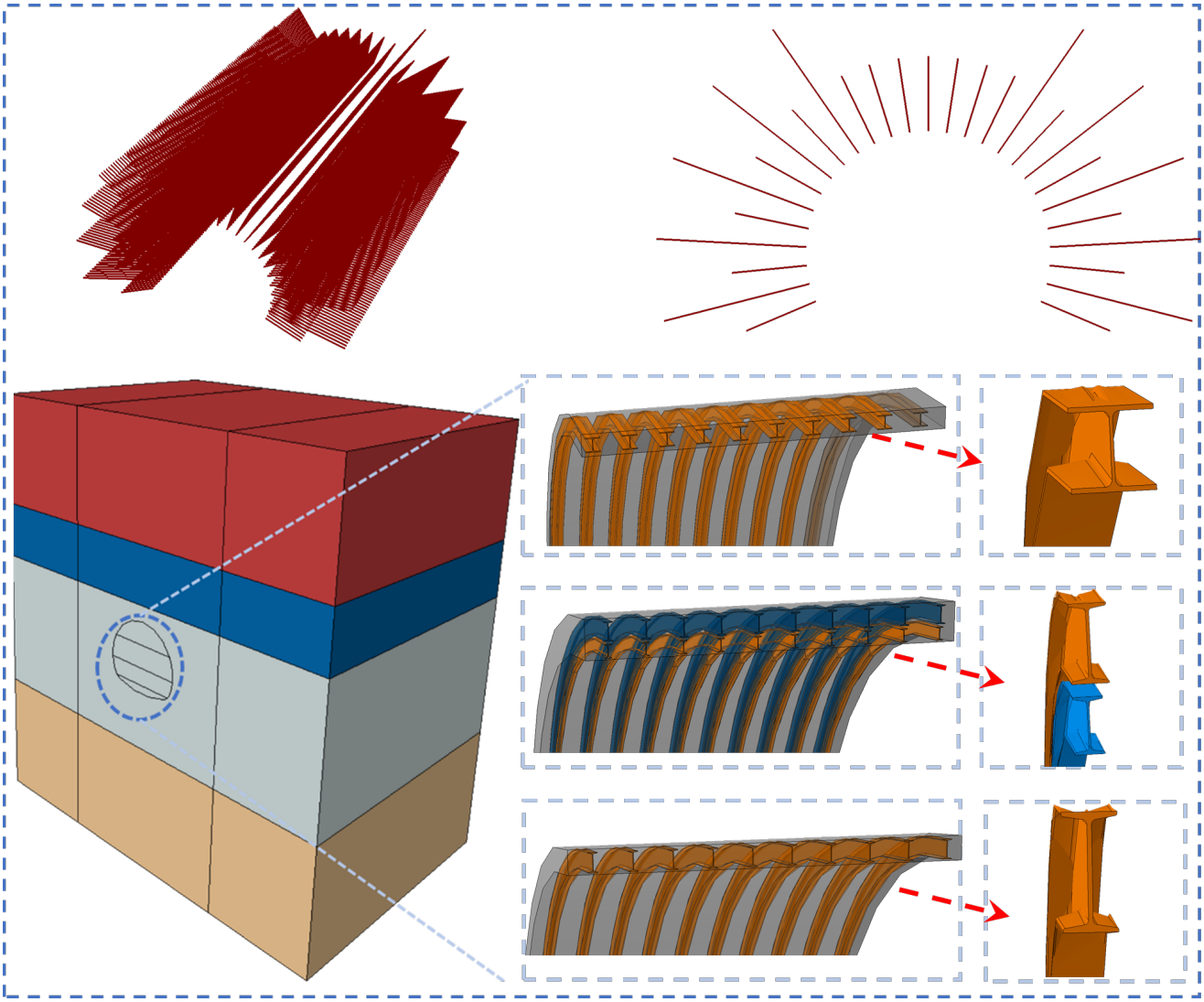

Fig. 6 Numerical calculation model for different support structure form

4 Numerical analysis of mechanical properties of different support structure

4.1 Numerical calculation model

According to the Saint Venant principle, the left and right boundaries of the model should be taken as 3–5 times the excavation span. According to the tunnel design parameters, the tunnel section height is 12.5 m, the excavation span is 14.52 m, and based on this, a numerical calculation model is established with a horizontal width of 74 m, a height of 77 m, and a thickness of 50 m.

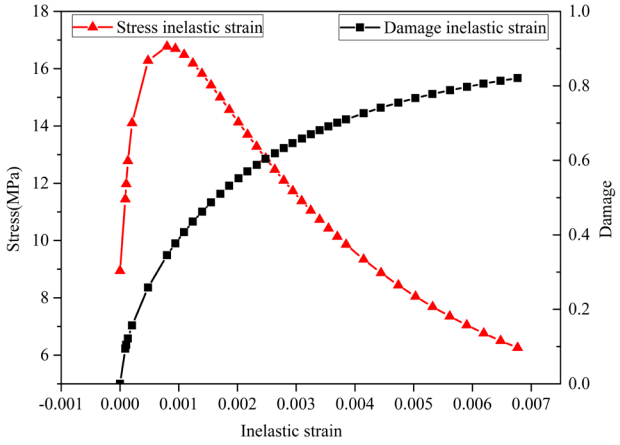

(a)

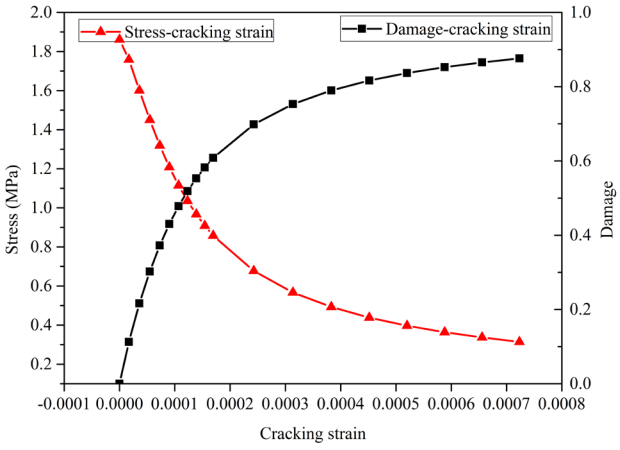

(b)

Fig. 7 Constitutive parameters of concrete CDP damage; (a) Compression damage curve, (b) Tensile damage curve

This study established a numerical calculation model for the combination of single-layer I-beams, single-layer H-beams, and double-layer I-beams. In the process of establishing the numerical model, the surrounding rock adopts a Mohr-Coulomb constitutive model, which is an ideal elastic-plastic structure. The primary support includes shotcrete, steel ribs, longitudinal connecting bars, and steel mesh. Longitudinal connecting bars and steel mesh are not considered in the numerical model. In this model, both shotcrete and steel rib are simulated using solid elements, and the cross-sectional shape and spatial position of the steel rib structure are strictly modeled based on the dimensions of the steel rib and its relative relationship with shotcrete in actual engineering. The numerical calculation models under different support structure forms are shown in Fig. 6.

To characterize the damage and failure behavior of shotcrete structures under compression and tension, the CDP damage coefficient of concrete was introduced in this study, and the compression and tensile damage coefficients are shown in Fig. 7. At the same time, the plastic parameters of the steel rib structure were also introduced to analyze the failure mechanism of the steel rib under large bending deformation. The physical and mechanical parameters of the surrounding rock and various components in the numerical model are shown in Table 1.

4.2 Distribution characteristics of bending moment and axial force in support structures

To reduce the influence of model boundary effects, this study obtained the results at the middle section position of the model, and the bending moment and axial force distribution of the steel rib and shotcrete structure from the tunnel vault to the tunnel invert are shown in Fig. 8.

Table 1 Physical and mechanical parameters

Part	Gravity/kg·m^{-3}	Elastic modulus /GPa	Poisson's ratio	Cohesion /kPa	Internal friction angle	Yield stress /MPa	Yield strain
Soil-1	2400	0.085	0.32	25	23	/	/
Soil-2	2350	0.105	0.32	36	28	/	/
Soil-3	2700	0.079	0.31	32	25	/	/
Soil-4	2850	0.115	0.31	30	30	/	/
Shotcrete	2200	25	0.32	/	/	/	/
Bolt	7850	206	0.2	/	/	200.2/246/294	0/0.0235/0.0474
Steel Rib	7850	206	0.2	/	/	200.2/246/294	0/0.0235/0.0474

From the distribution of axial force in different parts of the structure in Fig. 8 (a), it can be seen that the concrete in the upper parts of the structure is mainly compressed, while the lower part of the structure gradually turns into tensile force under uplift deformation. At the same time, in the upper part of the structure, under external compression, the axial force distribution of shotcrete and steel rib structures is relatively uniform and the transition is relatively smooth. However, in the lower part of the structure, the changes in axial force between the two structures are more severe. Therefore, in soft rock tunnels mainly characterized by vertical deformation, the upper part of the structure is mainly under pressure, while the lower part of the structure is mainly under axial tension and there are many stress concentration areas.

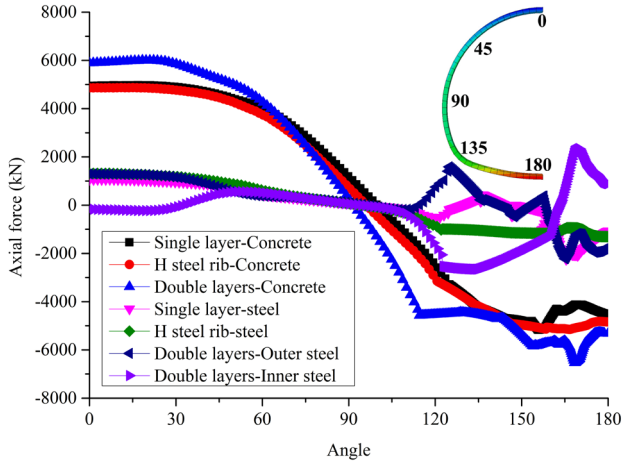

(a)

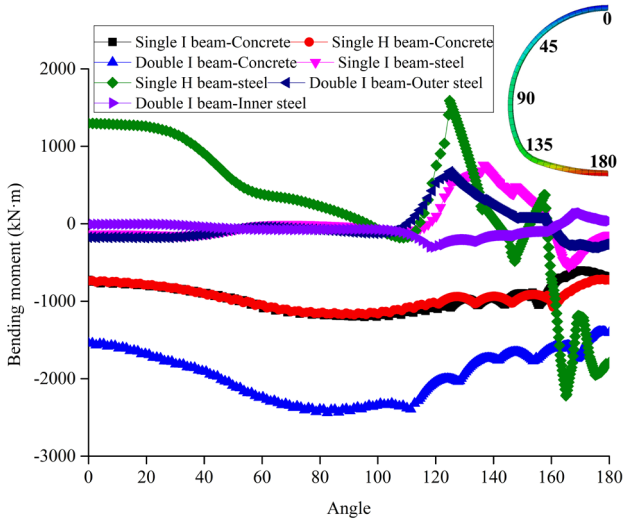

(b)

Fig. 8 Internal force distribution under different support structure forms; (a) Axial force, (b) Bending moment

The direction of the negative bending moment is clockwise, from Fig. 8 (b), it can be concluded that all parts of shotcrete have a certain degree of bending deformation towards the tunnel inside, and there are many stress concentration areas in the lower part of the structure, which are prone to local instability and damage. Similar to the distribution form of concrete bending moment, the bending moment distribution of each steel rib structure in the upper part of the tunnel is relatively uniform. For different support forms, there is a large fluctuation for structure internal force in the lower part, and stress concentration is prone to occur in the lower part of the primary support structure, which is prone to structural damage and instability failure. Compared with steel rib structures, the axial force and bending moment of shotcrete structures are larger under various working conditions.

4.3 Analysis of damage and mechanical characteristics of support structures

4.3.1 Damage characteristics of sprayed concrete structures

In large deformation tunnels, shotcrete in various parts may undergo different mechanical responses and damage failures due to differences in structural internal forces and bearing modes. This study further obtained the damage distribution of shotcrete in various parts under different support structure forms, as shown in Fig. 9.

From Fig. 9 (b), it can be seen that the concrete at various positions under different working conditions is mainly under compression, and the compressive stress shows a trend of increasing first and then decreasing from the tunnel vault to the tunnel invert. The maximum compressive stress is mainly concentrated at the arch waist and arch foot positions. Compared with the concrete stress at the upper part of the tunnel, the stress fluctuation at the tunnel invert is more severe, and there are many stress concentration areas, which also leads to a sharp fluctuation of concrete compression damage and plastic strain at the tunnel invert, as shown in Fig. 9 (a) and Fig. 9 (c). Compared to H-beam and single-layer I-beam support, the stress at each position of the concrete in the double-layer I-beam support structure is generally smaller, and the magnitude and fluctuation of concrete compression damage and plastic strain are generally smaller. The structure only undergoes local plastic yielding in the lower part, and the value of compression damage in most parts of the structure is relatively small.

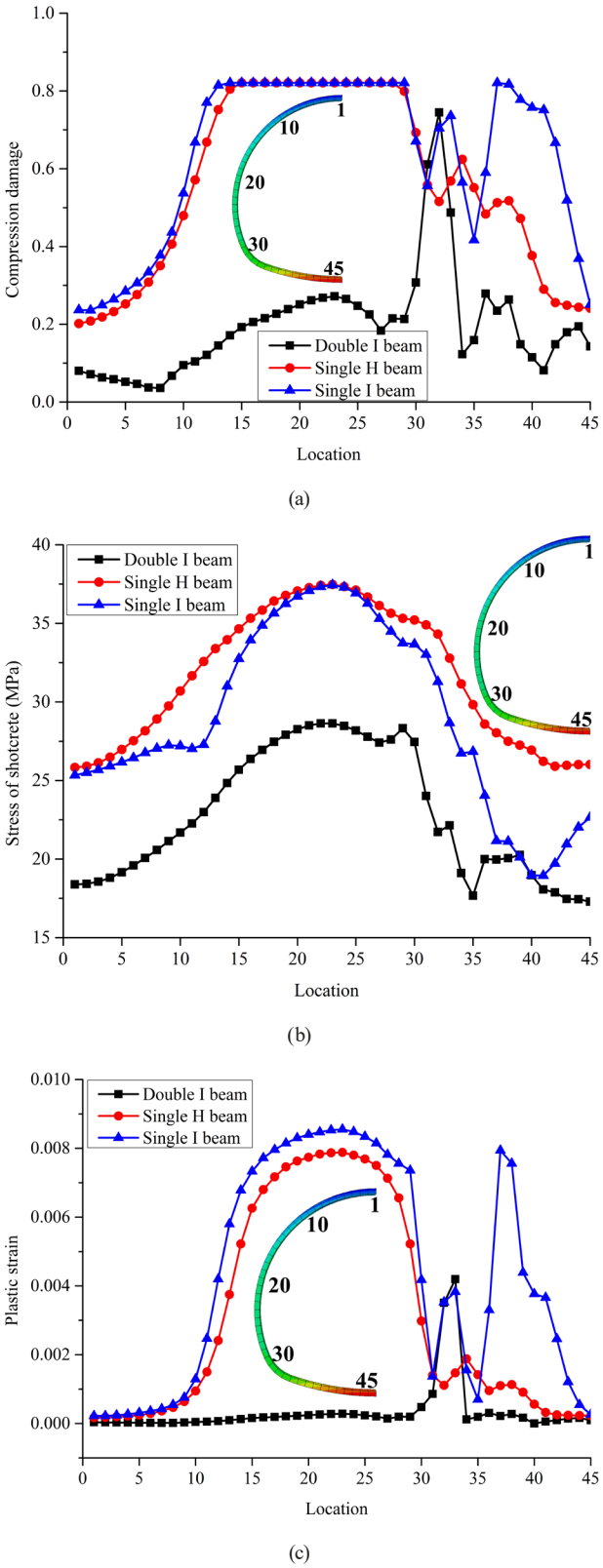

Fig. 9 Concrete damage and stress distribution under different support forms; (a) Compression damage, (b) Concrete stress, (c) Plastic strain of concrete

4.3.2 Mechanical characteristics of steel rib structure

H-beam and I-beam are both rib-shaped irregular structures with larger bearing surfaces at both ends and smaller bearing surfaces in the middle, which makes the steel rib structure prone to uneven bending deformation under external loads, resulting in significant differences in stress distribution between the inner and outer sides of the steel rib. Under the action of larger external loads, the steel rib structure is often in an ultimate bearing state and the deformation distribution is uneven, resulting in the steel rib structure often in an eccentric compression state. The stress distribution on the inner and outer sides of the steel rib structure under different support combinations is shown in Fig. 10.

From Fig. 10, it can be seen that under the H-shaped steel and single-layer I-shaped steel, The overall stress of the steel rib at each position from the tunnel vault to the

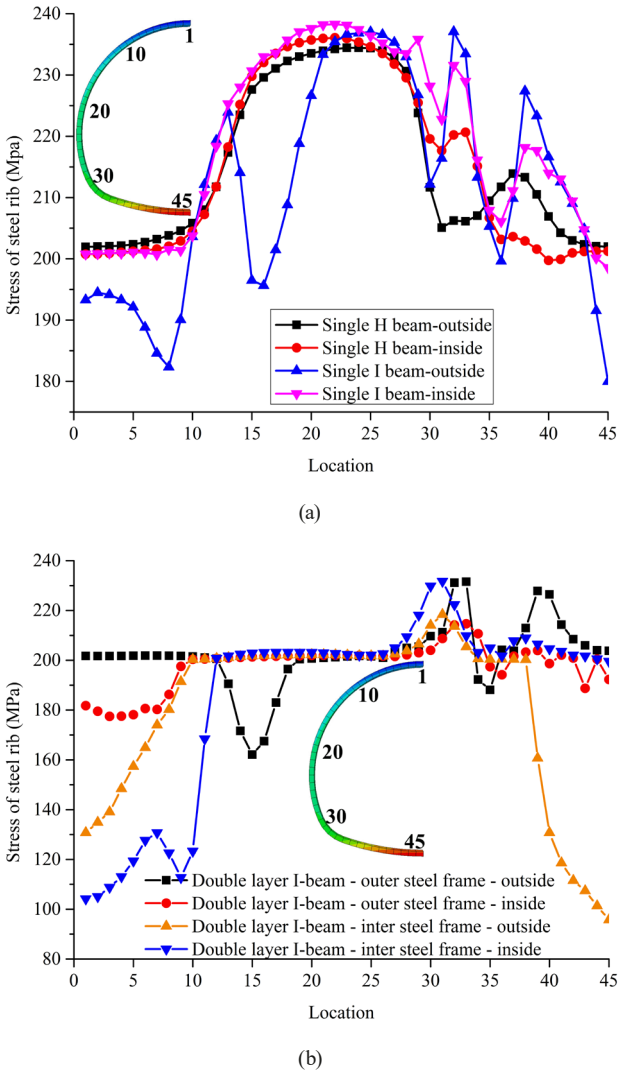

Fig. 10 Stress distribution on the inner and outer sides of steel rib; (a) Single-layer steel rib, (b) Double-layer steel rib

tunnel invert shows a trend of increasing and then decreasing, and the internal and external stresses of each type of steel fluctuate sharply at the tunnel invert. It can be concluded that the steel rib structure plays a main load-bearing role at the arch waist and arch foot, and there are many stress concentration areas in the steel rib structure at the tunnel arch foot and tunnel invert. For single-layer steel rib, the stress distribution on the inner and outer sides of H-shaped steel is more uniform than that of I-shaped steel, and the stress changes at each position are more gradual. However, there are many stress concentration areas on the inner and outer sides of I-shaped steel structures, and the stress difference between the inner and outer sides is large. The entire structure is in an eccentric bearing state, which is prone to significant bending instability deformation, and the overall safety and stability of the structure are low.

For the double-layer I-beam structure support, the internal and external stresses of the inner and outer steel ribs fluctuate sharply at the tunnel vault and tunnel invert, while the stress changes at the arch waist and arch foot positions are relatively gentle. The variation pattern of the inner and outer steel stresses at each position is consistent. In terms of the stress magnitude of the steel rib at each position, the overall stress of the outer steel rib is greater than that of the inner steel rib, and there is a significant difference in stress at the tunnel vault and tunnel invert. It can be concluded that the outer steel rib plays the main load-bearing role at the above two positions.

4.3.3 Bearing characteristics of primary support structure

The main contact between the primary support and the surrounding rock is the shotcrete structure, and the overall mechanical characteristics of the primary support structure are directly related to the external surrounding rock load borne by the shotcrete. The contact pressure and deformation between shotcrete and surrounding rock under different support structures are shown in Fig. 11.

From the comparative analysis of Fig. 11, it can be seen that the contact pressure between shotcrete and surrounding rock under different support structures is the highest at the tunnel arch foot, and the distribution characteristics from the tunnel vault to the tunnel invert first increase and then decrease. On the other hand, the deformation characteristics of tunnel shotcrete are opposite. The horizontal convergence deformation of shotcrete at the tunnel arch foot towards the tunnel is smaller than the settlement at the tunnel vault and uplift deformation at the tunnel invert. The double-layer support structure has a relatively high overall stiffness due to the combined bearing effect of the inner and outer steel ribs and can maintain small deformation characteristics under external loads, which means that there is a strong squeezing contact effect between the tunnel vault and the tunnel invert and the surrounding rock. The contact pressure at these two positions is relatively high, and the structural deformation is relatively small under high support stiffness.

Different forms of support structures not only present different bearing characteristics but also lead to differences in the mechanical state and deformation behavior of the surrounding rock. The stress distribution of the surrounding rock and the combined bearing effect of primary support under different support forms are shown in Fig. 12.

From Fig. 12 (a), it can be observed that, compared with single-layer structure and H-shaped steel structure, the plastic strain and stress of the surrounding rock under the double-layer steel rib composite structure are relatively small overall, and double-layer steel rib structure can effectively reduce the plastic strain and stress magnitude of the surrounding rock, which can effectively improve the stress state of the surrounding rock. Based on Fig. 12 (b), it can be concluded that the stress and plastic strain of H-beam and single-layer I-beam structures are relatively large and widely distributed, and there are multiple stress concentrations and plastic-yielding positions in the structure, especially the plastic yielding of the structure mainly occurs at the arch waist and arch foot on both sides.

Compared with the two types of support mentioned above, the shotcrete structure in the double-layer I-beam composite support structure only experiences compression damage at the corner of the side wall, while the shotcrete

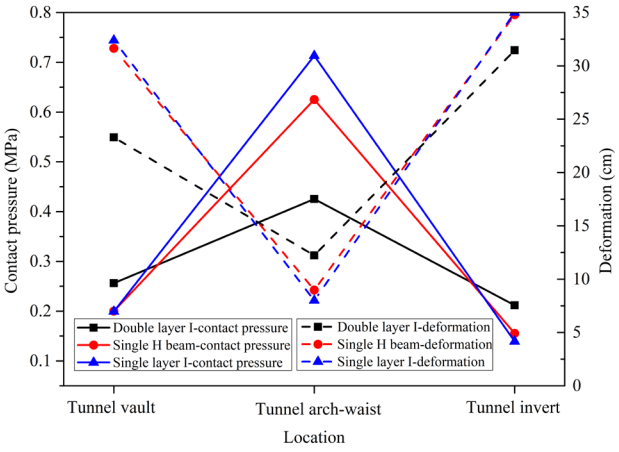

Fig. 11 Distribution of external contact pressure and structural deformation of shotcrete

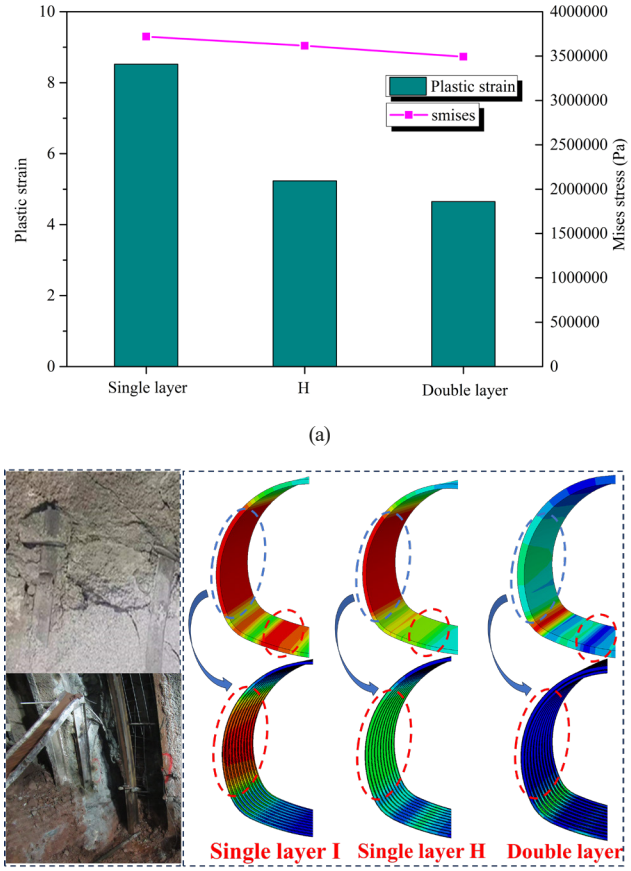

Fig. 12 The stress distribution of the surrounding rock and combined bearing effect of primary support; (a) Plastic strain and stress of surrounding rock (b) Joint bearing effect of support structure

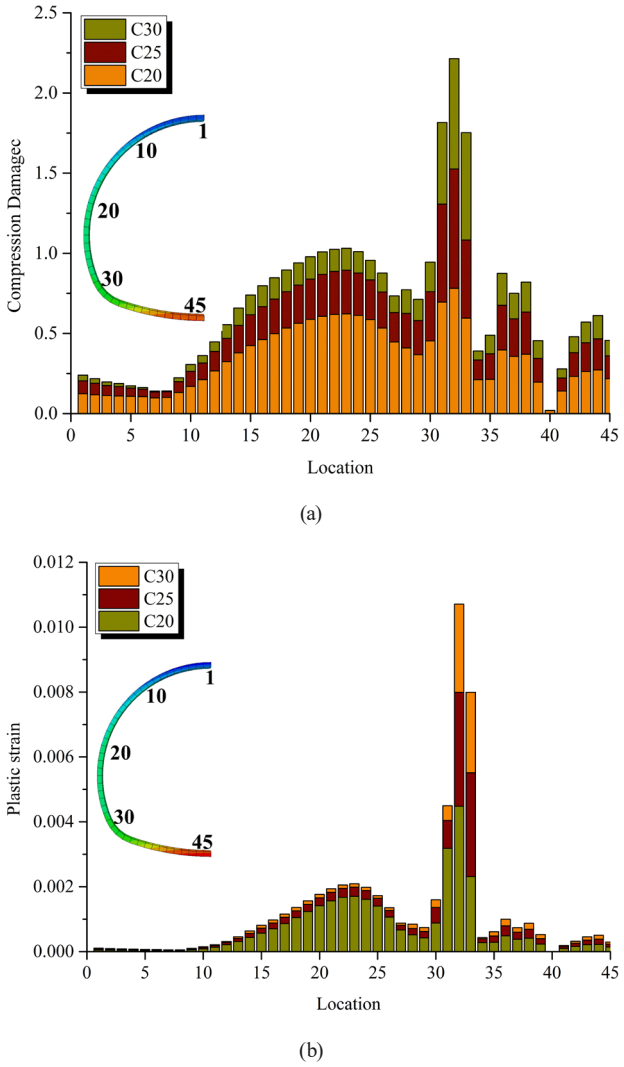

Fig. 13 Compressive damage and plastic strain of shotcrete under different shotcrete strengths; (a) Concrete compression damage, (b) Plastic strain in shotcrete

in other parts is in a relatively stable stress state. The combined support of the inner and outer steel rib structure results in a smaller plastic strain and smaller stress for the structure. The plastic strain value of the inner and outer steel rib is relatively small, and the combined structure only undergoes plastic yielding within a small range.

4.4 Structure mechanical properties under different shotcrete strength

The primary support of the tunnel is composed of the steel rib and the shotcrete layer. As a structure that directly contacts the surrounding rock and wraps the steel rib structure, the shotcrete's strength is crucial for the overall safety and stability of the tunnel structure. The distribution of compressive damage and plastic strain of concrete under different concrete strengths are shown in Fig. 13.

From Fig. 13, it can be seen that in tunnels with different shotcrete strengths, the compressive damage of the shotcrete from the tunnel vault to the tunnel invert shows a distribution characteristic of first increasing and then decreasing. The degree of concrete damage at the arch foot and side wall foot of the tunnel is greater than that at other positions, and the degree of concrete damage fluctuates sharply from the side wall foot to the tunnel invert. By comparing and analyzing the damage degree of shotcrete with different strengths, it can be concluded that in the lower part of the tunnel where the degree of concrete damage fluctuates greatly and is widely distributed, the difference in the damage degree between different concrete strengths is greater. In the upper part of the tunnel where the degree of damage is smaller, the difference between different calculation conditions is smaller.

The damage and cracking of sprayed concrete and the plastic yield of the steel rib structure are crucial to its structural performance and the long-term safety and stability of the tunnel structure. The primary support damage

and yield state under different sprayed concrete strengths are shown in Fig. 14, and the stress ratio on the inner and outer sides of the steel rib and the deformation of the primary supporting structure are shown in Fig. 15.

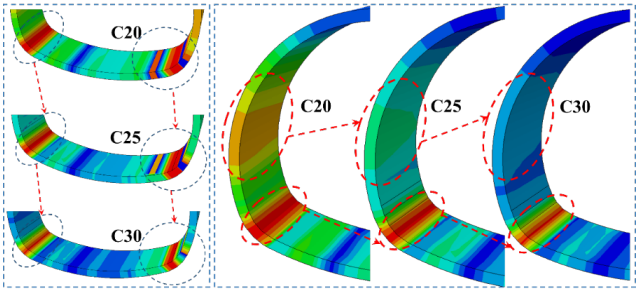

(a)

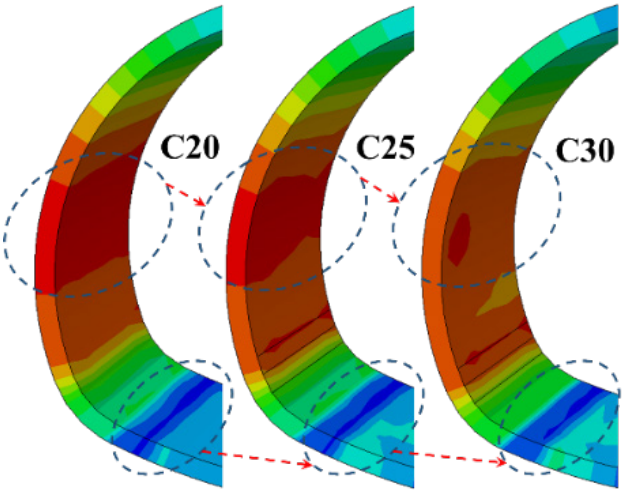

(b)

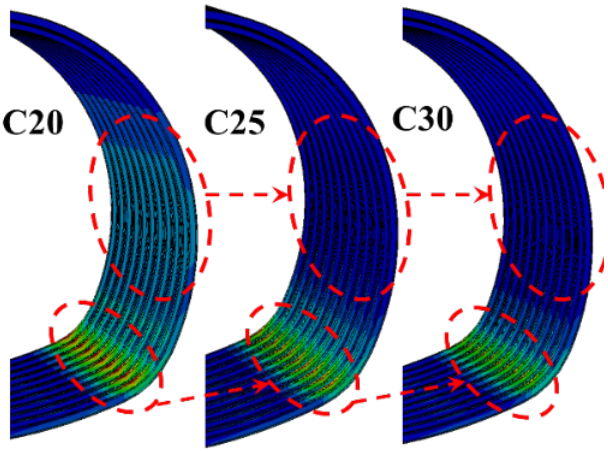

(c)

Fig. 14 Primary support damage and yield state under different shotcrete strengths; (a) Shotcrete compression damage, (b) Concrete stress distribution, (c) Plastic strain distribution of steel rib

From Fig. 14, it can be seen that different shotcrete strengths significantly impact the overall damage degree and stress state of the concrete structure. As the concrete strength gradually increases, the damage degree of the tunnel's lower parts and the arch waist gradually decreases, especially the distribution range of concrete damage at the sidewall foot significantly decreases. At the same time, it can be observed that as the strength of the concrete increases at the tunnel arch waist, the stress concentration state at the arch waist is improved, and the distribution of sprayed concrete stress at this position becomes more uniform. Especially for the primary support structures at the arch waist and sidewall foot with significant damage in the past, higher concrete strength can effectively improve the stress concentration state of the structure and reduce the compression damage and plastic yield range of the structure, thus maintaining high safety performance of the structure.

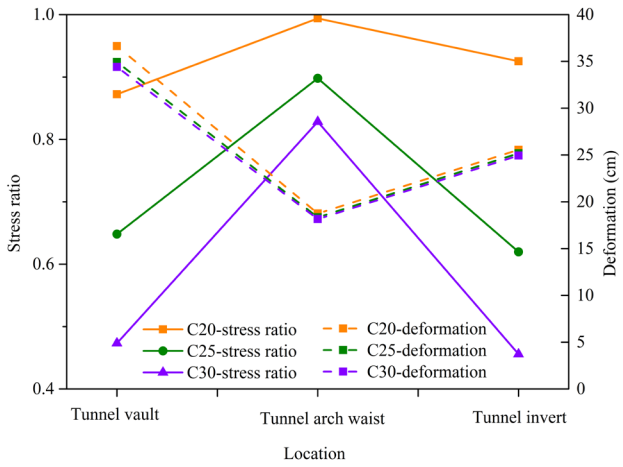

(a)

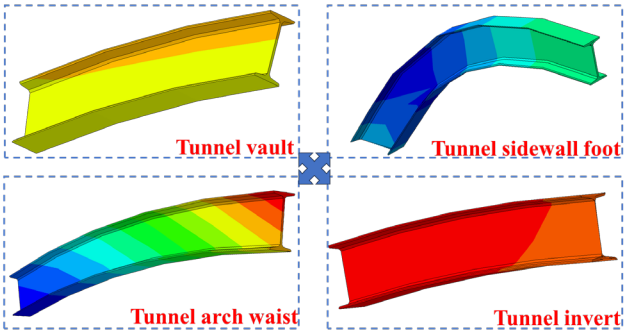

(b)

Fig. 15 Comparison of stress and deformation of primary support; (a) Comparison of deformation and stress ratio between inner and outer sides of shotcrete, (b) Comparison of internal and external stresses in various parts of a single-layer I-beam structure

From Fig. 15, it can be seen that the internal and external stress ratios of tunnel steel rib structures with different concrete strengths are the highest at the arch waist, while the arch crown and inverted arch are relatively small. Based on the stress and compression state of tunnel sprayed concrete mentioned above, there is significant compression damage at the arch waist of the tunnel, where the concrete structure undergoes significant plastic yielding and damage, resulting in a significant decrease in load-bearing performance. At this point, the inner and outer steel rib structures, as collaborative load-bearing parts, have played a significant bearing role, so the stress of the inner and outer steel rib structures is relatively high, and the difference between them is relatively small.

By comparing the internal and external stress ratios of steel rib structures under different concrete strengths, it can be found that the higher the concrete strength, the smaller the internal and external stress ratio. At the same time, the combined steel rib system composed of the inner and outer steel ribs, as mentioned in the previous analysis, is more used for safety reserves and supplementary bearing effects. Concrete structures with higher strength can share larger external loads. At this time, the combined steel rib system composed of inner and outer steel ribs shares smaller loads as a whole, and the stress of the inner and outer steel ribs is relatively small, indicating that compared to the outer steel rib, the overall stress of the inner steel rib structure is smaller. The outer steel rib in the combined steel rib system plays the main bearing effect, and the safety reserve performance of the inner steel rib is greater.

5 Conclusions

This study evaluated the structural failure mechanisms and structural mechanical response of different support forms in soft rock tunnels. The main research conclusions are as follows:

1. Compared with steel rib structures, the axial force and bending moment of sprayed concrete are relatively large under various working conditions. In the H-beam support and single-layer I-beam support conditions, the sprayed concrete mainly undergoes compression damage at the edges of the arch waists and arch feet on both sides, while in the double-layer I-beam support condition, the concrete only undergoes a certain degree of compression damage at the arch feet on both sides.
2. Compared with single-layer support structures, double-layer I-steel support structures have a more uniform stress distribution at various positions under the synergistic force of the inner and outer steel ribs, and there are relatively few stress concentration areas. In the double-layer I-beam composite support structure, the sprayed concrete only experiences compression damage at the corner of the side wall. The combined support of the inner and outer steel rib structure results in a smaller plastic strain and stress on the structure.
3. As the strength of sprayed concrete increases, the stress distribution of sprayed concrete at the arch waist becomes more uniform. At the same time, the stress concentration state of sprayed concrete at the corner of the tunnel wall and the plastic yield state of the steel rib structure have also been improved. Higher concrete strength can significantly reduce the stress of concrete and steel rib structure, especially for the primary support structure at the arch waist and corner of the tunnel sidewall with greater damage.

Acknowledgment

The project presented in this article is supported by the Henan Province Science and Technology Research Projects (No. 232102320029).

References

[1] Liu, W. W., Chen, J. X., Chen, L. J., Luo, Y. B., Shang, Q. C., Zhang, L. X., Gao, S. K., Jia, H. Y. "A rational construction method and deformation control system of tunnelling in extremely soft and fractured chlorite schist medium", Tunnelling and Underground Space Technology, 143, 105472, 2024. https://doi.org/10.1016/j.tust.2023.105472

[2] Zhou, J. G., Qiu, D. C., Sun, S. Q., Zhou, H., Chen, D. Y., Chen, H., Hu, H. J., Hu, H. C. "Settlement Prediction Method of Extra-Large Diameter Tunnels in Soft Rock Strata", Advances in Civil Engineering, 2023, 5558160, 2023. https://doi.org/10.1155/2023/5558160

[3] Tian, Y., Shu, X. Y., Tian, H. M., He, L. K., Jin, Y., Huang, M. "Effect of horizontal stress on the mesoscopic deformation and failure mechanism of layered surrounding rock masses in tunnels", Engineering Failure Analysis, 148, 107226, 2023. https://doi.org/10.1016/j.engfailanal.2023.107226

[4] Fan, X. M., Juang H., Wasowskic, J., Huang, R. Q., Xu, Q., Scaringi, G., Westen, C. J., Havenith, H. B. "What we have learned from the 2008 Wenchuan Earthquake and its aftermath: A decade of research and challenges", Engineering Geology, 241, pp. 25–32, 2018. https://doi.org/10.1016/j.enggeo.2018.05.004

[5] Feng, J. M., Tan, Y. M., Yao, S. Y., Jiang, H., Zhang, J. R., Li, H. T. "Study on stress variation of advance fiberglass anchor bolts during tunnel excavation process", Scientific Reports, 13(1), 4173, 2023. https://doi.org/10.1038/s41598-023-31000-4

[6] Sun, H. K., Gao, Y., Fang, Z. D., Chen, Y., Yang, Y. L. "Full-Scale Rotary Cutting Experimental Study and Development of Prediction Formulas for TBM Cutting Force", Arabian Journal for Science and Engineering, 48(10), pp. 13353–13376, 2023. https://doi.org/10.1007/s13369-023-07805-w

[7] Manh, H. T., Sulem, J., Subrin, D., Billaux, D. "Anisotropic Time-Dependent Modeling of Tunnel Excavation in Squeezing Ground", Rock Mechanics and Rock Engineering, 48(6), pp. 2301–2317, 2015. https://doi.org/10.1007/s00603-015-0717-y

[8] Li, Y. J., Zhang, D. L., Fang, Q., Yu, Q. C., Xia, L. "A physical and numerical investigation of the failure mechanism of weak rocks surrounding tunnels", Computers and Geotechnics, 61, pp. 292–230, 2014. https://doi.org/10.1016/j.compgeo.2014.05.017

[9] Wu, H., Fan, F. F., Yang, X. H., Wang, Z. C., Lai, J. X., Xie, Y. L. "Large deformation characteristics and treatment effect for deep bias tunnel in broken phyllite: A case study", Engineering Failure Analysis, 135, 106045, 2022. https://doi.org/10.1016/j.engfailanal.2022.106045

[10] Guo, X. P., Jiang, A. N. "Study on Applicability of Double Layer Superimposed Primary Support Arch Cover Method for Large-Span Station in Upper Soft and Lower Hard Stratum", KSCE Journal of Civil Engineering, 26(3), pp. 1407–1418, 2021. https://doi.org/10.1007/s12205-021-0538-3

[11] Chen, Z. Q., He, C., Wang, J., Ma, C. C. "Time-dependent squeezing deformation mechanism of tunnels in layered soft-rock stratum under high geo-stress", Journal of Mountain Science, 18(5), pp. 1371–1390, 2021. https://doi.org/10.1007/s11629-020-6356-0

[12] Liu, W. W., Chen, J. X., Luo, Y. B., Chen, L. J., Shi, Z., Wu, Y. F. "Deformation Behaviors and Mechanical Mechanisms of Double Primary Linings for Large-Span Tunnels in Squeezing Rock: A Case Study", Rock Mechanics and Rock Engineering, 54(5), pp. 2291–2310, 2021. https://doi.org/10.1007/s00603-021-02402-5

[13] Wu, K., Shao, Z. S., Jiang, Y. Z., Zhao, N. N., Qin, S., Chu, Z. F. "Determination of Stiffness of Circumferential Yielding Lining Considering the Shotcrete Hardening Property", Rock Mechanics and Rock Engineering, 56(4), pp. 3023–3036, 2023. https://doi.org/10.1007/s00603-022-03122-0

[14] Li, G., Ma, F. S., Guo, J., Zhao, H. J., Liu, G. "Study on deformation failure mechanism and support technology of deep soft rock roadway", Engineering Geology, 264, 105262, 2019. https://doi.org/10.1016/j.enggeo.2019.105262

[15] Wu, K., Song, J. N., Zhao, N. N., Shao, Z. S. "Study on the time-dependent interaction between surrounding rock and yielding supports in deep soft rock tunnels", International Journal for Numerical and Analytical Methods in Geomechanics, 48(2), pp. 566–587, 2023. https://doi.org/10.1002/nag.3650

[16] Sun, F. X., Jin, Z., Wang, C., Gou, C., Li, X., Liu, C., Yu, Z. "Case Study on Tunnel Settlement Calculations During Construction Considering Shield Disturbance", KSCE Journal of Civil Engineering, 27(5), pp. 2202–2216, 2023. https://doi.org/10.1007/s12205-023-0925-z

[17] Tao, Z. G., Zhao, F., Wang, H. J., Zhang, H. J., Peng, Y. Y. "Innovative constant resistance large deformation bolt for rock support in high stressed rock mass", Arabian Journal of Geosciences, 10(15), 341, 2017. https://doi.org/10.1007/s12517-017-3127-5

[18] Sun, Z. , Zhang, D., Hou, Y., Huangfu, N., Li, M., Guo, F. "Support Countermeasures for Large Deformation in a Deep Tunnel in Layered Shale with High Geostresses", Rock Mechanics and Rock Engineering, 56(6), pp. 4463–4484, 2023. https://doi.org/10.1007/s00603-023-03297-0

[19] Liu, W., Chen J., Luo Y., Chen L., Zhang L., … Dong F. "Long-term stress monitoring and in-service durability evaluation of a large-span tunnel in squeezing rock", Tunnelling and Underground Space Technology, 127, 104611, 2022. https://doi.org/10.1016/j.tust.2022.104611

[20] Zhang, J., Gao, S., Yang, T., He, Y., Wu, J., Wu, H. "Study of the Failure Mechanism of Soft Rock Mining Roadways Based on Limit Analysis Theory", Applied Sciences, 13(18), 10323, 2023. https://doi.org/10.3390/app131810323

[21] Sun, N., Li, X. K., Li, S. G., Hu, D. K., Hu, M. J., Zhang, F. M., Zhong, Y. Y., Dong, M. L., Li, Z. N. "The Deformation Law of a Soft-Rock Cavern by Step Excavation in a Pumped Storage Power Station", Applied Sciences, 13(15), 8970, 2023. https://doi.org/10.3390/app13158970

[22] Yang, Y., Meng, L., Zhang, T. "Full Anchor Cable Support Mechanism and Application of Roadway with Thick Soft Rock Mass Immediate Roof", Applied Sciences, 13(12), 7148, 2023. https://doi.org/10.3390/app13127148